Theoretical Aspects of the Heterobimetallic Dimers with the *T over Square* Structural Motif. Synthesis and Structure of a Heteronuclear Platinum and Palladium Complex with 1-Methylcytosinato Bridging Ligands

Carlo Mealli,*[1a] Fabio Pichierri,[1b] Lucio Randaccio,*[1b] Ennio Zangrando,[1b] Michael Krumm,[1c] Dagmar Holtenrich,[1c] and Bernhard Lippert*[1c]

Istituto per lo Studio della Stereochimica ed Energetica dei Composti di Coordinazione, CNR, 50132 Florence, Italy, Dipartimento di Scienze Chimiche, Università di Trieste, 34127 Trieste, Italy, and Fachbereich Chemie, Universität Dortmund, D-44221 Dortmund, Germany

Received June 16, 1994[⊗]

The molecular structure of *trans*-$[(NH_3)_2Pt(\mu\text{-}1\text{-}MeC^-)_2Pd(NH_3)]$ $[Pd(NH_3)_4]_{0.5}(NO_3)_3\cdot 3H_2O$ (**1**) has been determined by X-ray crystallography. The compound crystallizes in the triclinic space group $P\bar{1}$ (No. 2), with $a = 7.476(2)$ Å, $b = 11.373(3)$ Å, $c = 16.397(4)$ Å, $\alpha = 87.27(2)°$, $\beta = 85.32(2)°$, $\gamma = 88.74(2)°$, and $Z = 2$. The structure was refined to $R = 0.034$ and $R_w = 0.038$ for 5045 independent reflections. The complex is best described by a square planar coordination of Pd and a square pyramidal one of Pt with the Pd in the apical position (*T over square geometry, TSQ*). The Pt and Pd atoms are bridged by two nearly coplanar 1-methylcytosinate anions with a Pt−Pd distance of 2.511(1) Å. A theoretical analysis, based on EHMO calculations, highlights the nature of the single M−M′ bond in d^8−d^8 dimers of this type (4:3) and points out the correlations with the better known d^8−d^8 dimers (4:4) characterized by two parallel square planar coordination geometries. The M−M′ bond order in the latter is close to zero, but not null. Finally, the fate of the M−M′ linkage for adding one or two electrons to the above *TSQ* species is formally analyzed. A correlation is made with the structural data available for dimers with d^8−d^9 and d^8−d^{10} electron counts [*e.g.* Pt(II)−Cu(II) and Pt(II)−Hg(II) species with bridging nucleobases]. While one additional electron weakens the M−M′ linkage without destroying the primary *TSQ* geometry, two extra electrons force the expulsion of the ligand formerly coaxial with the metals (4:2 adducts). The M−M′ interaction in the 4:2 adducts is comparable with that proposed for the 4:4 species.

Introduction

Dinuclear complexes of type *cis*-$[X_2M(\mu\text{-}L)_2M'Y_2]^{n+}$, containing the d^8 metal ions M = M′ = Pt(II) or Pd(II), or M = Pt(II) and M′ = Pd(II), and difunctional bridging ligands μ-L, as well as additional ligands X,Y (usually NH_3, amines, or halogens) have been extensively studied.[2] The main structural feature of these complexes is that they are built up with the metal coordination planes facing each other (Chart 1a).

The corresponding *trans*-isomers are not obtainable, probably because of the severe steric hindrance between X and Y ligands. In fact, the small bite of the μ-L ligands and their reciprocal arrangement seem to prevent even a small tilt of the L_4M planes which could relieve the problem (Chart 1b). A way to avoid the steric clash is the isomerization to the corresponding *cis*-complex, as observed in *cis*-$[(NH_3)_2Pd(\mu\text{-}1\text{-}MeC^-)_2Pd(NH_3)_2]^{2+}$ (where 1-MeC^- = 1-methylcytosinate) formed from two *trans*-$(NH_3)_2Pd(II)$ entities.[3] Otherwise, d^8−d^8 dinuclear complexes of the *trans* type are obtainable upon the loss of one monodentate ligand. Thus, compounds of formula *trans*-$[X_2Pt(\mu\text{-}L)_2PdY]^{n+}$, where μ-L = (μ-1-MeC^-), have been isolated and structurally characterized.[4] In these compounds the two metal coordination planes are perpendicular to each other, with Pt acting as a ligand for Pd and *vice versa* (Chart 1c). While the mutually perpendicular orientation of two d^8 metal ions is not unprecedented,[5−7] these dinuclear Pt(II), Pd(II) cytosine com-

Chart 1

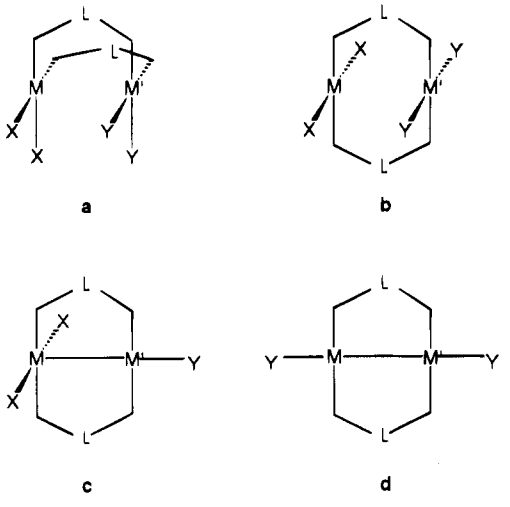

⊗ Abstract published in *Advance ACS Abstracts,* May 15, 1995.

(1) (a) CNR, Florence. (b) University of Trieste. (c) University of Dortmund.

(2) (a) Lippert, B. *Prog. Inorg. Chem.* **1989**, *37*, 1. (b) Matsumoto, K.; Moriyama, H.; Suzuki, K. *Inorg. Chem.* **1990**,*29*, 2096. (c) Micklitz, W.; Renn, O.; Schollhorn, H.; Thewalt, U.; Lippert, B. *Inorg. Chem.* **1990**, *29*, 1836. (d) O'Halloran, T. V.; Lippard, S. J. *Inorg. Chem.* **1989**, *28*, 1289. (e) Matsumoto, K.; Miyamae, H.; Moriyama, H. *Inorg. Chem.* **1989**, *28*, 2959. (f) Micklitz, W.; Riede, J.; Huber, B.; Muller, G.; Lippert, B. *Inorg. Chem.* **1988**, *27*, 1979.

(3) Krumm, M.; Mutikainen, I.; Lippert, B. *Inorg. Chem.* **1991**, *30*, 884.

(4) (a) Krumm, M.; Lippert, B.; Randaccio, L.; Zangrando, E. *J. Am. Chem. Soc.* **1991**, *113*, 5129. (b) Krumm, M.; Zangrando, E.; Randaccio; L. Menzer, S.; Lippert, B. *Inorg. Chem.* **1993**, *32*, 700.

(5) Haines, R. J.; Meintjes, E.; Laing, M. *Inorg. Chim. Acta* **1979**, *36*, L403.

(6) (a) Frew, A. A.; Manojlovic Muir, L.; Muir, K. W. *J. Chem. Soc. Chem. Commun.* **1980**, 624. (b) Brown, M. P.; Cooper, S. J.; Frew, A. A; Manojlovic Muir, L.; Muir, K. W.; Puddephatt, R. J.; Seddon, K. R.; Thomson, M. A. *Inorg. Chem.* **1981**, *20*, 1500.

(7) Arena, C. G.; Ciani, G.; Drommi, D.; Faraone, F.; Proserpio, D. M.; Rotondo, E. *J. Organomet. Chem.* **1994**, *484*, 71.

0020-1669/95/1334-3418$09.00/0

plexes appear to be unique with respect to both the extreme shortness of the Pt−Pd bond (about 2.50 Å) and the fact that a similar bonding pattern has never been observed in nucleobase coordination chemistry. Comparable short bonds (2.50−2.70 Å) are reported in dinuclear Pt(I), Pt(I),[8] Pd(I), Pd(I),[9] and Pt-(I), Pd(I)[10] complexes, where the metal coordination planes are likewise coplanar and linked by two bridging ligands μ-L (Chart 1d). Most reasonably, a covalent single metal−metal bond can be invoked for the latter complexes in Chart 1d. The nature of the Pt−Pd linkage in *trans*-$[X_2Pt(\mu\text{-}L)_2PdY]^{n+}$ is likely different, and the formalism of a dative $Pt^{II}\rightarrow Pd^{II}$ bond, resulting from the overlap of a filled d_{z^2} with an empty $d_{x^2-y^2}$ orbital, was qualitatively proposed.[4] A similar formalism was reported for a few organometallic diplatinum complexes.[6,7,11]

More recently, by using the same ligand system extended to μ-L = 1,5-dimethylcytosinate (μ-1,5-DimeC$^-$), d^8-d^9 [Pt(II)−Cu(II)][12] and d^8-d^{10} [Pt(II)−Hg(II)][13] dinuclear compounds have been prepared and structurally characterized. While the former d^8-d^9 species have the same framework as the d^8-d^8 ones, there is no monodentate ligand, coaxial with the M−M′ vector, in the Hg adduct. In any case, these more electron rich dimers have comparatively long intermetallic distances (Pt−Hg, about 2.8 Å, and Pt−Cu, about 2.5 Å), a result which is also supported by ^{195}Pt NMR spectra.[13]

During studies on Pt, Pd complexes with chelating nucleobases, a compound with a C_{10}/N_{14} ratio was obtained which was initially considered a trinuclear species. The subsequent crystal structure analysis revealed a compound of formula *trans*-$[(NH_3)_2Pt(\mu\text{-}1\text{-}MeC^-)_2Pd(NH_3)]$ $[Pd(NH_3)_4]_{0.5}(NO_3)_3\cdot 3H_2O$ (**1**), with the presence of a binuclear complex of type *trans*-$[X_2Pt(\mu\text{-}1\text{-}MeC^-)_2PdY]^{n+}$, and of a discrete tetraammine−palladium-(II) cation, $[Pd(NH_3)_4]^{2+}$. Since the same binuclear cation was already structurally characterized[4] in *trans*-$[(NH_3)_2Pt(\mu\text{-}1\text{-}MeC^-)_2Pd(NH_3)](NO_3)_2$ (**2**), it seems of interest to evaluate whether the presence of the large cation $[Pd(NH_3)_4]^{2+}$, as well as the different number of nitrate anions, may affect the geometry of the dimer and the Pt−Pd distance, in particular. Beside these experimental aspects, the present paper addresses the relationships between the type of structural framework, the overall electron population, and the extent of the intermetallic interaction in terms of the theoretical arguments derivable from extended Hückel molecular orbital (EHMO) calculations[14] and the fragment molecular orbital (FMO) formalism.[15]

Table 1. Atomic Fractional Coordinates and Equivalent Isotropic Temperature Factors (Å^2) of **1**

atom	x	y	z	B_{eq}[a]
Pt	0.01104(4)	0.24861(2)	0.20219(2)	2.229(4)
Pd1	0.06848(7)	0.17969(5)	0.05901(3)	2.541(9)
Pd2	0.000	0.500	0.500	2.88(1)
O2	−0.1757(8)	0.4541(5)	0.2808(3)	3.7(1)
N1	−0.3213(8)	0.5481(6)	0.1800(4)	3.5(1)
N3	−0.1373(7)	0.3831(5)	0.1539(4)	2.6(1)
N4	−0.0781(8)	0.3183(6)	0.0227(4)	3.2(1)
C1	−0.405(1)	0.6312(8)	0.2370(7)	5.0(2)
C2	−0.2100(9)	0.4608(6)	0.2082(5)	2.8(1)
C4	−0.1582(9)	0.3942(6)	-0.0714(4)	2.7(1)
C5	−0.271(1)	0.4886(7)	0.0442(5)	3.8(2)
C6	−0.349(1)	0.5605(7)	0.0991(6)	3.8(2)
O2a	0.1140(9)	0.1690(5)	0.3676(3)	4.2(1)
N1a	0.3118(9)	0.0167(6)	0.3457(4)	3.9(1)
N3a	0.1664(8)	0.1104(5)	0.2388(4)	2.7(1)
N4a	0.2090(9)	0.0455(5)	0.1065(4)	3.2(1)
C1a	0.355(2)	0.0121(9)	0.4310(6)	6.1(2)
C2a	0.194(1)	0.1009(6)	0.3199(5)	3.3(1)
C4a	0.2446(9)	0.0353(6)	0.1833(5)	2.8(1)
C5a	0.366(1)	−0.0529(7)	0.2128(5)	4.0(2)
C6a	0.397(1)	−0.0577(7)	0.2911(5)	4.1(2)
N2	0.133(1)	0.1297(6)	−0.0578(4)	3.9(1)
N11	−0.2147(8)	0.1511(5)	0.2257(4)	3.0(1)
N12	0.2375(8)	0.3479(5)	0.1856(4)	2.9(1)
N21	0.191(1)	0.4152(7)	0.5642(4)	4.1(1)
N22	0.099(1)	0.4227(7)	0.3961(4)	4.3(2)
N7	0.4323(9)	0.8268(6)	−0.0339(4)	3.5(1)
O71	0.465(1)	0.8189(7)	0.0384(4)	6.3(2)
O72	0.3437(9)	0.9119(6)	−0.0578(5)	5.9(2)
O73	0.485(1)	0.7514(7)	−0.0809(5)	8.1(2)
N8	0.107(1)	0.6625(6)	0.2117(4)	4.1(1)
O81	0.162(1)	0.6029(6)	0.1535(4)	5.8(2)
O82	0.141(1)	0.6363(8)	0.2818(4)	6.9(2)
O83	0.016(1)	0.7520(7)	0.1974(5)	7.4(2)
N9	0.449(1)	0.6832(8)	0.6191(5)	5.4(2)
O91	0.5110(9)	0.6966(8)	0.6853(5)	6.5(2)
O92	0.327(1)	0.7497(8)	0.5989(5)	7.8(2)
O93	0.504(1)	0.6028(8)	0.5740(5)	8.4(2)
OW1	0.017(1)	0.1747(7)	0.5381(5)	7.1(2)
OW2	0.146(1)	0.0892(7)	0.6900(5)	6.5(2)
OW3	0.326(1)	0.7184(8)	0.4210(5)	8.2(2)

[a] Values for anisotropically refined atoms are given in the form of the isotropic equivalent displacement parameter defined as: $B_{eq} = (4/3)\sum_i\sum_j a_i a_j \beta(i,j)$.

Table 2. Relevant Bond Lengths (Å) and Angles (deg) with Esd's in Parentheses

Pt−Pd1	2.511(1)	Pd1−N4	1.996(6)
Pt−N3	2.037(5)	Pd1−N4a	1.997(6)
Pt−N3a	2.031(6)	Pd1−N2	2.042(7)
Pt−N11	2.040(6)	Pd2−N21	2.041(7)
Pt−N12	2.048(6)	Pd2−N22	2.032(7)
Pd1−Pt−N3	87.1(2)	N3a−Pt−N12	88.5(2)
Pd1−Pt−N3a	87.3(2)	N11−Pt−N12	176.7(3)
Pd1−Pt−N11	93.3(2)	Pt−Pd1−N4	87.3(2)
Pd1−Pt−N12	89.9(2)	Pt−Pd1−N4a	87.2(2)
N3−Pt−N3a	174.4(2)	Pt−Pd1−N2	175.7(2)
N3−Pt−N11	90.2(2)	N4−Pd1−N4a	174.5(3)
N3−Pt−N12	90.7(2)	N4−Pd1−N2	93.3(3)
N3a−Pt−N11	90.9(2)	N4a−Pd1−N2	92.2(3)
N21−Pd2−N22	90.5(3)		

Results and Discussion

Description of the Structure. Atomic coordinates of compound **1** are reported in Table 1 and selected bond lengths and angles in Table 2. A perspective view[16] and labeling scheme of the cations *trans*-$[(NH_3)_2Pt(\mu\text{-}1\text{-}MeC^-)_2Pd(NH_3)]^{2+}$

(8) (a) Manojlovic Muir, L.; Muir, K. W.; Solomun, T. *Acta Crystallogr., Sect. B* **1979**, *35*, 1237. (b) Fisher, J. R.; Mills, A. J.; Sumner, S.; Brown, M. P.; Thomson, M. A.; Puddephatt, R. J.; Frew, A. A.; Manojlovic Muir, L.; Muir, K. W. *Organometallics* **1982**, *1*, 1421. (c) Khan, Md. N. I.; King, C.; Wang, J.-C.; Wang, S.; Fackler, J. P. Jr. *Inorg. Chem.* **1989**, *28*, 4656. (d) Yip, H.-K.; Che, C.-M.; Peng, S.-M. *J. Chem. Soc. Dalton Trans.* **1993**, 179.

(9) (a) Holloway, R. G.; Penfold, B. R.; Colton, R.; Mc Cormic; R. J. *J. Chem. Soc., Chem. Commun.* **1976**, 485. (b) Uson, R.; Fornies, F.; Navarro, R.; Tomas, M.; Fortuno, C.; Cebollada, J. I.; Welch, A. J. *Polyhedron* **1989**, *8*, 1045. (c) Xie, Y.; Lee, C.-L.; Yang, Y.; Rettig, S. J.; James, B. R. *Can. J. Chem.* **1992**, *70*, 751.

(10) (a) Fornies, J.; Martinez, F.; Navarro, R.; Redondo, A.; Tomas, M.; Welch, A. J. *J. Organomet. Chem.* **1986**, *316*, 351. (b) Suzuki, T.; Iitaka, N.; Kurachi, S.; Kita, M.; Kashivabara, K.; Ohba, S.; Fujita, J. *Bull. Chem. Soc. Jpn.* **1992**, *65*, 1817.

(11) Lin, M.; Fallis, K. A.; Anderson, G. K.; Rath, N. P.; Chiang, M. Y. *J. Am. Chem. Soc.* **1992**, *114*, 4687.

(12) Fusch, G.; Hillgeris, E. C.; Lippert, B. *Abstracts from ESF Workshop: Metal Ion Interactions with Nucleic Acids and their Constituents*; University of Dortmund: Dortmund, Germany, 1993.

(13) Krumm, M.; Zangrando, E.; Randaccio, L.; Menzer, S.; Danzmann, A.; Holthenrich, D.; Lippert, B. *Inorg. Chem.* **1993**, *32*, 2183.

(14) Hoffmann, R.; Lipscomb, W. N. *J. Chem. Phys.* **1962**, *36*, 2179; **1962**, *37*, 3489. Hoffmann, R. *J. Chem. Phys.* **1963**, *39*, 1397.

(15) Albright, T. A.; Burdett, J. K.; Whangbo, M.-W. *Orbital Interactions in Chemistry;* John Wiley and Sons: New York, 1985.

(16) Johnson, C. K. *ORTEP*; Report ORNL-3794; Oak Ridge National Laboratory: Oak Ridge, TN, 1965.

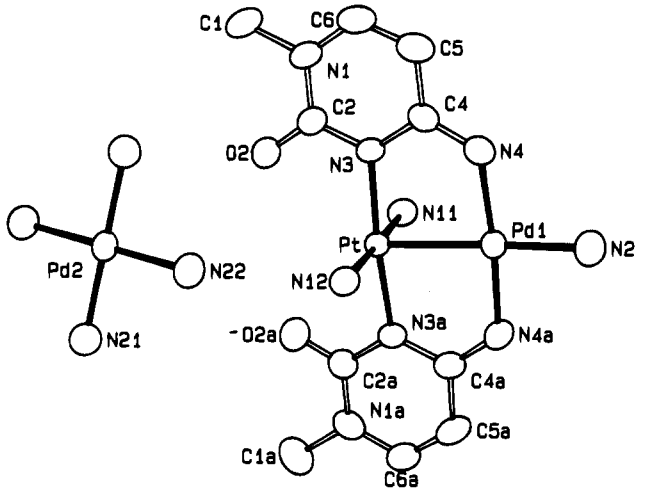

Figure 1. ORTEP drawing (thermal ellipsoid; 50% probability) and labeling scheme for cations of **1**.

and $[Pd(NH_3)_4]^{2+}$ is depicted in Figure 1. In the latter, the Pd lies on a crystallographic center of symmetry. In the dinuclear cation the Pd is square planar coordinated, whereas Pt is approximately square pyramidal with the heterometal in the apical position. The dihedral angle between the coordination plane of Pd and the basal plane of Pt is 86.4(1)°.

The metals are bridged by two almost parallel cytosinate anions through the endocyclic N3 and the deprotonated amino group, N4, in a *head*-to-*head* arrangement (Figure **1**), the dihedral angle between the cytosinate mean planes being 4(2)°. The metal−metal distance of 2.511(1) Å is close to that found in the same cation of (**2**) and falls within the range from 2.492(3) to 2.521(1) Å observed[4] in the cations *trans*-$[X_2Pt(\mu\text{-}1\text{-}MeC^-)_2PdY]^{n+}$, X = NH_3 or $MeNH_2$, varying the Y ligand at Pd, namely Cl^-, SCN^-, pyrazine, 1-methyluracil anion. The moiety Pt−(N3−C4−N4)$_2$−Pd is slightly bowed at the Pt and Pd centers as shown by the N3−Pt−N3a and N4−Pd−N4a angles (Table 2). The basal coordination plane of Pt has a slight tetrahedral distortion, with displacements of N_4 donors from the mean plane by ±0.078(6) Å and of Pt by 0.021 Å.

The Pd1−NH_3 distance of 2.042(7) is significantly longer than that of 2.001(5) Å reported[4] for the cation of (**2**), but very close to the Pd−NH_3 bond length of 2.039(3) Å found[3] in the *trans*-$[Pd(NH_3)_2(1\text{-}MeC)_2]^{2+}$ and to the two crystallographically independent Pd2−NH_3 distances of 2.041(7) and 2.032(7) Å in the cation $[Pd(NH_3)_4]^{2+}$. The crystal packing comparison of **1** and **2** indicates that the hydrogen bonding schemes involving NH_3 bonded to Pd in the dinuclear cation are very similar. Therefore, we are not able to explain the observed difference in the Pd−NH_3 distances. In $[(NH_3)_2Pt(\mu\text{-}1\text{-}MeC^-)_2PdCl]^+$,[4] the Pd−Cl distance of 2.313(1) Å is very close to the mean (2.298(9) Å) of 44 Pd−Cl bond lengths in $[PdCl_4]^{2-}$ anions retrieved from the Cambridge Structural Database.[17] This comparison, both for Pd−NH_3 and Pd−Cl distances, strongly suggests that Pt exerts a weak *trans*-influence, probably close to that of NH_3 and Cl^-.

The source of the $[Pd(NH_3)_4]^{2+}$ species in **1** is not fully clear. Almost certainly, we can rule out that *trans*-$[Pd(NH_3)_2Cl_2]$, used in the preparation of the aqua species, was contamined with poorly soluble $[Pd(NH_3)_4][PdCl_4]$, which in turn was used as the starting material for *trans*-$[Pd(NH_3)_2Cl_2]$. Rather, we feel that the solution behavior of *trans*-$[(NH_3)_2Pd(H_2O)_2]^{2+}$, which by ^{15}N NMR spectroscopy[18] has been demonstrated to rapidly disproportionate to mono- and triammine species, could also lead to some tetrammine species.

Chart 2

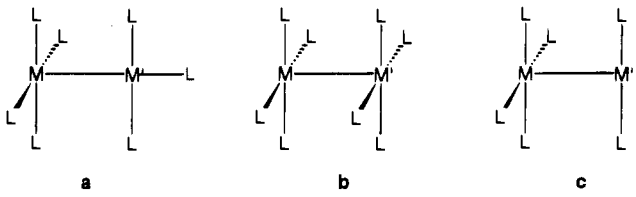

Table 3. Intermetallic Distances and Conformations in $L_4M-M'L_3$ Complexes with Electronic Configuration d^8-d^n (n = 8,9)

formula[a]	M−M′ (Å)	conf[b]	ref
$[Cl_2Rh(\mu\text{-etdp})_2Rh(CO)]$	2.661[c]	s	5
$[Rh(\mu\text{-pnp})_2Rh(CO)]^{2+}$	2.674(1)	s	19
$[(1,2\text{-}O_2C_6Cl_4)Rh(\mu\text{-dppm})_2Rh(CO)]$	2.637(1)	s	20
$[(MeCN)_2Rh(\mu\text{-tdpm})Rh(CO)_2]^{2+}$	2.745(1)	e	21
$[Cl(CO)Rh(\mu\text{-bzta})_2Pt(PPh_3)]$	2.6266(4)	e	22
$[Me_2Pt(\mu\text{-dppm})_2PtMe]^+$	2.769(1)	s	6
$[MeClPt(\mu\text{-}Ph_2Ppy)_2Pt(COMe)]^+$	2.728(3)	s	7
$[(NH_3)_2Pt(\mu\text{-}1\text{-}MeC^-)_2PdCl]^+$	2.518(1)	e	4
$[(NH_3)_2Pt(\mu\text{-}1\text{-}MeC^-)_2Pd(1\text{-}MeU^-)]^+$	2.515(1)	e	4
$[(NH_3)_2Pt(\mu\text{-}1\text{-}MeC^-)_2Pd(NH_3)]^{2+}$	2.511(1)	e	4
$[(NH_3)_2Pt(\mu\text{-}1\text{-}MeC^-)_2Pd(NH_3)]^{2+}$	2.511(1)	e	this work
$[(MeNH_2)_2Pt(\mu\text{-}1\text{-}MeC^-)_2Pd]_2(pyz)^{4+}$	2.492(3)	e	4
$[(MeNH_2)_2Pt(\mu\text{-}1\text{-}MeC^-)_2Pd(SCN)]^+$	2.521(1)	e	4
$[(MeNH_2)_2Pt(\mu\text{-}1\text{-}MeC^-)_2Cu(NH_3)]^{2+}$	2.556(3)	e	12[d]
$[(MeNH_2)_2Pt(\mu\text{-}1\text{-}MeC^-)_2Cu]_2(CO_3)^{2+}$	2.500(4)[e]	e	12
$[(MeNH_2)_2Pt(\mu\text{-}1\text{-}MeC^-)_2Cu(9\text{-}EtGH)]^{2+}$	2.5005(2)	e	12

[a] etdp = $(PhO)_2PN(Et)P(OPh)_2$; pnp = 2-[bis (diphenylphosphino)methyl]pyridine; dppm = bis(diphenylphosphino)methane; tdpm = tris(diphenylphosphino)methane; bzta = benzothiazole-2-thiolate; Ph_2Ppy = 2-(diphenylphosphino)pyridine; 1-MeC^- = 1-methylcytosinate; 1-MeU^- = 1-methyluracilate; pyz = pyrazine; 9-EtGH = 9-ethylguanine. [b] Conformation: s = staggered; e = eclipsed. [c] Esd not reported. [d] The Cu atom is involved in a weak interaction with a water molecule at 2.32(2) Å. [e] Mean value.

Molecular Orbital Analysis. $L_4M-M'L_3$ dimers of d^8 metal ions with the structural motif shown in Chart 2a (*T over square* = *TSQ*) are known,[4-7,19-22] and Table 3 summarizes the compounds which have been structurally characterized. It appears that the square planar L_4M unit, which formally contains 16 electrons and which could be stable as an isolated complex, is engaged in a significant axial interaction with the T-shaped metal fragment $M'L_3$.

In the Pt, Pd heterobimetallic series with nucleobases (μ-1-MeC^-),[4] the intermetallic separation is short (ca. 2.50 Å) compared to those in other systems containing stronger σ-donors, especially at the $M'L_3$ fragment. For example, in $[Me_2Pt(\mu\text{-dppm})_2PtMe]^+$,[6] (dppm = diphenylphosphinomethane) the Pt−Pt bond is as long as 2.769(1) Å. In all cases, however, the distances are shorter than in the known d^8-d^8 adducts of the type $L_4M-M'L_4$, where the two square planar units are stacked parallel to each other (see Chart 2b). The minimum separation between the metals is >2.85 Å in the latter 4:4 species.[23] As mentioned, Pt_2, Pd_2, and Pt, Pd adducts of the latter type are also obtainable with two (μ-1-MeC^-) ligands in the *cis*

(17) Allen, F. H.; Davies, J. E.; Galloy, J. J.; Johnson, O.; Kennard, O.; Macrae, C. F.; Mitchell, E. M.; Mitchell, G. F.; Smith, J. M.; Watson, D. G. *J. Chem. Inf. Comput. Sci.* **1991**, *31*, 187. The search was limited to structures with $R \leq 0.075$.

(18) Appleton, T. G.; Hall, J. D.; Ralph, S. F.; Thompson, C. S. M. *Aust. J. Chem.* **1988**, *41*, 1425.

(19) Anderson, M. P.; Pignolet, L. H. *Organometallics* **1983**, *2*, 1246.

(20) Ladd, J. A.; Olmstead, M. M.; Balch, A. L. *Inorg. Chem.* **1984**, *23*, 2318.

(21) El-Amouri, H.; Bahsoun, A. A.; Fischer, J.; Osborn, J. A. *Angew. Chem., Int. Ed. Engl.*, **1987**, *26*, 1169.

(22) Ciriano, M. A.; Perez-Torrente, J. J.; Lahoz, F. J.; Oro, L. A. *Inorg. Chem.* **1992**, *31*, 969.

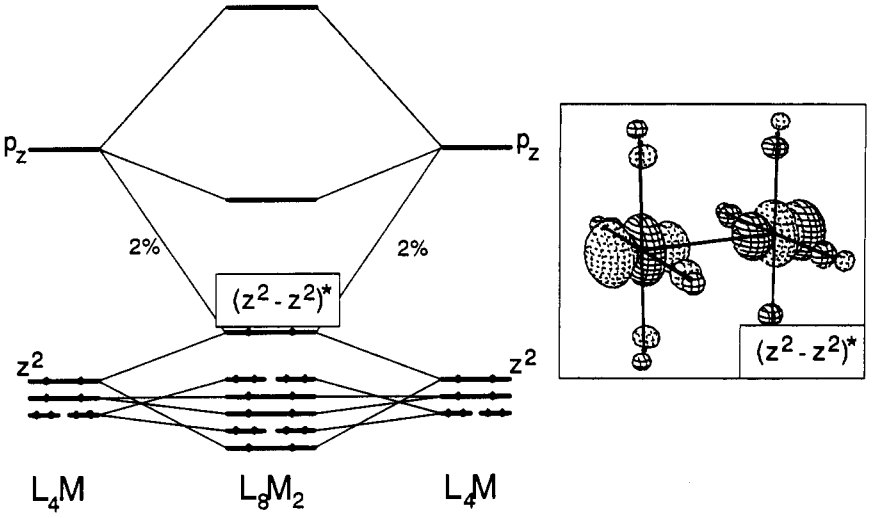

Figure 2. Molecular orbital diagram for $L_4M-M'L_4$ type compounds including the 3D drawing of the HOMO.

arrangement.[2] For convenience, we shall reconsider shortly the theoretical underpinnings of the M−M′ bonding in the 4:4 dimers.[24]

A square planar d^8 metal has attributable amphoteric character as the filled z^2 orbital exerts some basicity, while the coaxial and high lying p_z orbital carries potential Lewis acidity. Under these circumstances, two bidirectional but equivalent $z^2 \rightarrow p_z$ donor-acceptor interactions could be hypothesized for the species shown in Chart 2b. The pair of two-electron/two-orbital interactions (no matter how weak) would lead to the wrong inference that the M−M′ bond order is 2 in these dimers. Basic MO and symmetry arguments can easily elucidate the inadequacy of the latter statement which is also in contrast with the current theoretical ideas.[24]

The diagram shown in Figure 2 for a model $[(NH_3)_4Pt-Pt(NH_3)_4]^{4+}$ species shows that the two z^2 orbitals (slightly above three other non-bonding d orbitals) give rise to in-phase and out-of-phase σ-combinations which, being filled, would result in a significant four-electron repulsion between the metals. The p_z orbitals become important because their out-of-phase combination mixes somewhat into the HOMO, $(z^2 - z^2)^*$. Indeed, the phase of the mixing is such that not only the destabilization of the level is reduced but the z^2 lobes rehybridize in out-pointing directions. The latter effect is visible in the 3D drawing of the HOMO in spite of the small p_z contibution ($\leq$2%). Were the mixing becoming larger and larger, the HOMO would progressively lose its σ^* character and would eventually become a combination of out-pointing metal lone pairs. In summary, as soon as the contribution of the p_z orbitals is sufficiently large to balance or even overcome the repulsive effects between the z^2 orbitals, the M−M′ bond order becomes greater than zero.

The latter orbital mixing is not the only one which may affect a direct metal−metal bonding interaction. In agreement with some previous results,[24c] there is a significant contribution (at least 5%, not shown) of the metal s orbitals in both the σ and σ^* levels of Figure 2. In particular, the s orbital is found to outweigh the former *in-phase* combination in some Ni_2 and Pd_2 dimers with short intermetallic separations. Also, since the s orbital is in principle devoted to the formation of metal−ligand bonding, stronger M−M′ interactions are expected with weak σ-donors which do not excessively destabilize the atomic orbital in question (*vide infra*).

In summary, the z^2/p_z and z^2/s rehybridizations are the qualitative theoretical underpinnings for the slightly positive M−M′ interaction in 4:4 dimers. A bonding energy of ca. 9 kcal/mol, recently calculated at the *ab initio* level for some Pt(II) and Rh(I) species,[24d] seems very reasonable. In any case, the bond order remains closer to zero than to one, mainly because of the large gap between z^2 and p_z in metals such as Pd or Pt, which limits the propensity for rehybridization. Moreover, the stronger the σ-donor capabilities of the ligands, the smaller the residual s orbital contribution and the weaker the M−M′ interaction will be.

After this premise, useful for the subsequent discussion, we address the M−M′ bonding in the 4:3 dimers (Chart 2a).[4,6,7] The relatively short intermetallic distances cannot be due solely to the presence of binucleating ligands holding the two metals in place: important electronic factors must be operative. Initially, the simple model used was $[(NH_3)_4Pt-PdH_2(NH_3)]^{2+}$ where two *trans* Pd−H linkages, eclipsing two Pt−NH_3 bonds, were chosen so as to avoid steric clashes. On the other hand, the barrier for the rotation of the two fragments is almost insignificant at this computational level and a staggered conformation could have been adopted as well. The adoption of a more realistic model with two binucleating ligands of the type (μ-1-MeC^-) would not have affected the primary MO features, highlighted in Figure 3. On the left side of the latter, the well known frontier orbitals of square planar species (compare with Figure 2) consist of a total of four filled d orbitals. At higher energy, the p_z orbital is not far from the $x^2 - y^2$ orbital, which, destabilized by the equatorial ligands, is not shown. On the side of the T-shaped PdL_3 fragment, the orbital closer to the latter is indicated as being of the $x^2 - y^2$-type, although it is actually aligned along the z axis. Because of one missing equatorial ligand, the FMO in question does not only lie closer to the block of the four d orbitals but is also somewhat hybridized with p_y, thus pointing toward the Pt atom. The electronegativity difference between Pd and Pt accounts for the slight differences between the blocks of filled d orbitals as well as between the high lying pure p orbitals.

(23) Balch, A. L.; Catalano, V. J. *Inorg. Chem.* **1992**, *31*, 3934. This reference reports an useful summary of the intermetallic distances in the dinuclear systems, generally classified as *n:m*, according to the numbers *n* and *m* of L ligands around the two metallic centers. Accordingly, the species under observation and presented in Scheme 2 are 4:3, 4:4, and 4:2, respectively.

(24) (a) Mann, K. R.; Gordon, J. G., II; Gray, H. B. *J. Am. Chem. Soc.* **1975**, *97*, 3553. (b) Christoph G. G.; Koh Y.-B. *J. Am. Chem. Soc.* **1979**, *101*, 1422. (c) Cotton F. A.; Matusz M.; Poli R.; Feng X. *J. Am. Chem. Soc.* **1988**, *110*, 1144. (d) Novoa J. J.; Aullòn G., Alemany P., Alvarez S., submitted for publication.

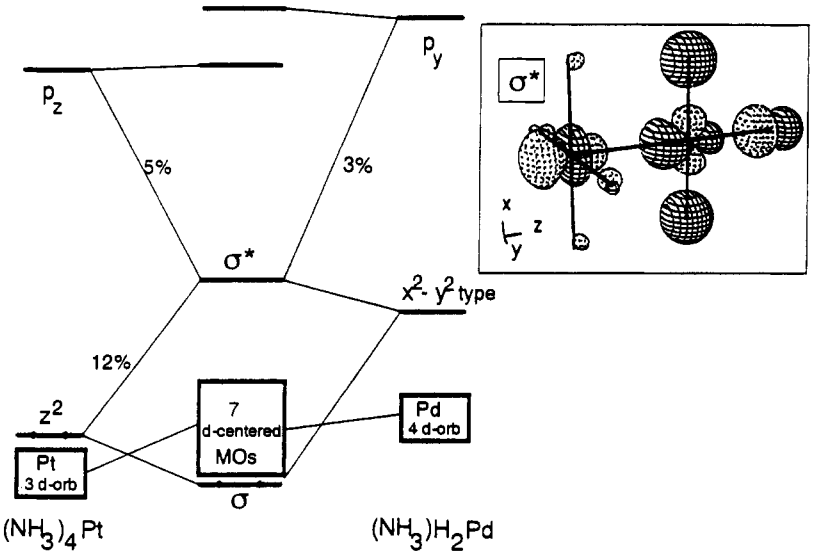

Figure 3. Molecular orbital diagram for the model compound $[(NH_3)_4PtPdH_2(NH_3)]^{2+}$ and the 3D drawing of the LUMO.

The strongest and practically unique interaction between the two fragments involves the Pt-z^2 and the Pd-$x^2 - y^2$-type FMOs. While the σ-bonding MO is part of the bulk of 7+1 filled d orbitals, the antibonding counterpart (σ^* = LUMO) is sufficiently separated (the calculated gap is >2 eV). Clearly, a two-electron/two-orbital donor–acceptor interaction is operative in this case and a formal M–M′ bond order of 1 can be assumed. It is interesting to compare the 3D drawing of the LUMO in Figure 3 with that of the HOMO of the $L_4M-M'L_4$ species in Figure 2. Both levels appear to be characterized by M–M′ antibonding. In both cases, the rehybridization with the p_z redirects a bigger lobe of the Pt-z^2 orbital (L_4M fragment) away from the M–M′ vector.[25] Conversely, the second metal is inwardly hybridized, although the direction can be reversed depending on the presence or absence of the coaxial ligand (4:3 or 4:2 species). This argument is important to understand some developments in the chemistry of these systems (*vide infra*) as there is a subtle interplay between the electronic population of σ^* and the acceptance or the ejection of one of the ligands.

In some of the known d^8-d^8 $L_4M-M'L_3$ species containing strong σ-donors (*e.g.* phosphines or alkyl groups) the M–M′ separation can be ca. 0.2–0.3 Å larger than in the analogous compounds containing the (μ-1-MeC^-) nucleobases (see Table 3). Comparative EHMO calculations were performed for the models $[(NH_3)_4Pt-Pt(NH_3)_3]^{4+}$ and $[Me_2(PH_3)_2Pt-Pt(PH_3)_2Me]^+$, the latter mimicking the compound $[Me_2Pt(\mu\text{-dppm})_2PtMe]^+$.[6] The numerical result is significant. In fact, by fixing a staggered $L_4M-M'L_3$ conformation and a constant Pt–Pt separation of 2.5 Å, the Pt–Pt overlap population decreases from 0.26 to 0.17 when the seven ammines are replaced by the stronger phosphine and methyl σ-donors. As mentioned for the 4:4 species (Chart 2b), a more destabilized metal s orbital at the square planar fragment limits the bonding capabilities toward the second metal. However, the presence of stronger donor substituents has the greatest effect at the $M'L_3$ fragment. As inferred by the diagram of Figure 3, the $x^2 - y^2$-type FMO, σ-antibonding with the terminal ligands, rises in energy, while the z^2 orbital of the fragment L_4M is barely affected. Eventually, the increased energy gap between the interacting FMOs accounts for a weaker interaction between the two metals, in agreement with the longer distance.

(25) The p_z contribution is larger in Figure 3 than in Figure 2 (5% vs 2%) because of the high destabilization which forces σ^* to get closer to p_z itself.

Another emerging point is that the energy of the σ^* MO (LUMO) is not too high for it to be populated (as mentioned, ca. 2eV above the HOMO in the Pt, Pd model, which is closest to the experimental structure). While the electrochemical behavior of the Pt(II)–Pd(II) species on reduction remains to be explored, a conceptual way of adding electrons to the system is the introduction of more electron rich metal ions [*e.g.*, a stepwise replacement of Pd(II) with Cu(II) and Cu(I)]. Remarkably, heterodinuclear Pt(II)–Cu(II) complexes of the type $L_4M-M'L_3$, containing the difunctional ligand (μ-1-MeC^-), were synthesized, and their structural determination[12] confirms that the primary geometry in Chart 2a is preserved. Even if the Cu orbitals (and the CuL_3 FMOs as well) are lower in energy with respect to the Pd analogs, the basic σ interaction, shown in Figure 3, is still important. The σ^* level, now singly populated (SOMO) has similar features, although lying closer to the block of filled d orbitals (the gap is only ca. 1eV, in this case). The coexistence of a filled σ-bonding MO with a half-filled σ^* partner reduces the formal M–M′ bond order to 0.5 (or to zero, were the level σ^* doubly populated). On the other hand, the Pt(II)–Cu(II) bond in the known *TSQ* structures (ca. 2.5 Å) is practically equal to the shortest bonds in d^8-d^8 dimers (see Table 3).

In this latter regard, consider that a direct comparison between pairs of different metals is not fully appropriate. Moreover the halving of the formal M–M′ bond order does not affect dramatically the corresponding distance as shown by comparative calculations for a given Pt, Pd system with variable electron count. Only a stepwise 15% decrease of the Pt, Pd overlap population is observed in the models $[(NH_3)_4Pt-Pd(NH_3)_3]^{4+,3+,2+}$ with fixed geometry (d^8-d^8, d^8-d^9 and d^8-d^{10} species, respectively). A rationale for such a trend is found by looking again at the drawing of σ^* in Figure 3. Besides being M–M′ antibonding, the MO is antibonding with the terminal ligands primarily on the side of the $M'L_3$ fragment (not surprising for a $x^2 - y^2$ orbital in square planar coordination). As confirmed by the trends for the overlap population, one or two electrons populating the MO in question weaken the M′–L_{ax} bonds more significantly than the M–M′ one. Recall again that the z^2 orbital of L_4M is already hybridized away from $M'L_3$. Moreover, if the M′–L_{ax} bond is elongated, the inward metal hybridization at $M'L_3$, disfavoring the M–M′ bond, disappears or is even reverted outward when L_{ax} is eventually removed from the system (see Figure 4).

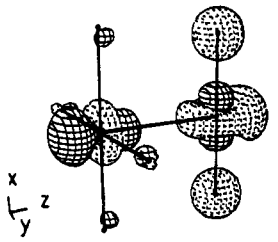

Figure 4. 3D drawing of the HOMO for $L_4M-M'L_2$ type compounds.

Table 4. Intermetallic Distances and Conformations in $L_4M-M'L_2$ Complexes with Electronic Configuration d^8-d^{10}

formula[a]	M−M′ (Å)	conf[b]	ref
$[(CO)(PPh_3)_2Ir(\mu\text{-}MeN_3ptol)Ag(iba)]$	2.874(2)	e	26
$[(CO)(PPhMe_2)_2Ir(\mu\text{-}MeN_3Me)CuCl]$	2.686(3)	e	27
$[Cl(CO)Ir(\mu\text{-}dppm)_2Au]^+$	2.986(1)	e	28
$[(CNMe)_2Ir(\mu\text{-}dppm)_2Au]^+$	2.944(1)	e	29
$[(CO)(PPh_3)_2Rh(\mu\text{-}MeN_3Me)CuCl]$	2.730(3)	e	30
$[Rh(\mu\text{-}pnp)_2Au]^+$	2.850(2)	s	31
$[(CN)_2Pt(\mu\text{-}dppm)_2Au]^+$	3.046(2)	e	32
$[(C{\equiv}CPh)_2Pt(\mu\text{-}dppm)_2Au]^+$	2.910(1)	e	33
$[(MeNH_2)_2Pt(\mu\text{-}1\text{-}MeC^-)_2Hg]^{2+}$	2.785(1)	e	13[c]
$[(MeNH_2)_2Pt(\mu\text{-}1\text{-}MeC^-)_2Hg]^{2+}$	2.765(1)	e	13[c]
$[(MeNH_2)_2Pt(\mu\text{-}1,5\text{-}DimeC^-)_2Hg]^{2+}$	2.835(1)	e	13[c]

[a] MeN_3ptol = methyl(*p*-tolyl)triazenido; iba = isobutyric acid; MeN_3Me = dimethyltriazenido; 1,5-DimeC$^-$ = 1,5-dimethylcytosinate; for other abbreviations see Table 3. [b] Conformation: e = eclipsed; s = staggered. [c] The X-ray structures of these adducts show that there are residual bonding capabilities in other directions not coaxial with the Pt−Hg vector. Usually, two additional interactions departing from the Hg atom are long and appear more ionic than covalent in character.

As a matter of fact, if a d^9 metal is replaced by a d^{10} one, [Cu(I), Au(I), or Hg(II)] the only stable complexes known have the structure of type $L_4M-M'L_2$ (4:2) shown in Chart 2c, *i.e.* a long M−M′ linkage seems to survive (see Table 4) whereas L_{ax} is definitely lost.[13,26−33] Interestingly, all of the compounds of Table 4 are supported by the presence of two binucleating ligands.

The progressive weakening and expulsion of a ligand as a consequence of the electron population of a σ^* MO (such as that in Figure 3) is not novel. A similar trend has been observed and discussed by some of us[34] relative to a series of d^8 and d^{10} monomeric nickel complexes containing the tripodal ligand np_3 [np_3 = $N(CH_2CH_2PPh_2)_3$]. The trigonal bipyramidal structure of $[(np_3)NiX]^{2+}$ (X = halide) is mantained in the monocationic derivative, although axially elongated. The halide ligand is definitelly expelled in the last member of the series, *i.e.* the trigonal pyramidal complex $[(np_3)NiX]^0$. Structural and electrochemical evidence has been provided in this case.

The last point to be addressed is whether there is still some effective M−M′ bond in the $L_4M-M'L_2$ compounds (Chart 2c). Metal ions such as Au(I) and Hg(II) are known to be stable as isolated $M'L_2$ species with linear geometries. There is a known analogy between these 14 electron species and the classical square planar 16 electron complexes, because of the fact that two, not just one, p metal orbitals stay uninvolved in bonding at high energy. In these terms, the analogy can be extended to show that the $L_4M-M'L_2$ adducts adapt to a bonding scheme quite similar to that illustrated above for the $L_4M-M'L_4$ species (Chart 2b).

Two z^2 orbitals, both filled, give rise to in-phase and out-of-phase combinations. The metals would be ultimately repulsive to each other, if there were no mixing of the high p orbitals in the $(z^2 - z^2)^*$ combination. The drawing in Figure 4 (to be compared with that in Figure 2) shows a clear-cut outward rehybridization of the z^2 orbitals which may be sufficient to switch the M−M′ repulsion into a weak attraction and possibly raises the M−M′ bond order above zero. Moreover the metal s orbitals may provide an important contribution to bonding. To confirm experimentally that $L_4M-M'L_4$ and $L_4M-M'L_2$ species adapt the same atypical M−M′ bonding scheme, the two types of structures, containing the same M−M′ pair must be available. Unfortunately, the available data, summarized in Table 4 and in ref 23, do not allow such a comparison.

Table 5. Crystallographic Data and Details of Refinements of **1**

formula	$C_{10}H_{27}N_{14}O_{11}Pd_{1.5}Pt \cdot 3H_2O$
fw	928.15
a, Å	7.476(2)
b, Å	11.373(3)
c, Å	16.397(4)
α, deg	87.27(2)
β, deg	85.32(2)
γ, deg	88.74(2)
V, Å^3	1387.7(6)
D(calcd), g cm^{-3}	2.22
Z	2
space group	$P\bar{1}$ (No. 2)
μ, cm^{-1}	61.2
F(000)	900
radiation	Mo Kα (λ = 0.7107 Å)
2θ max	56
abs cor	ψ scan
octants collcd	$\pm h, \pm k, +l$
no. of reflcns measd	6899
no. of indep reflcns [$I > 3\sigma(I)$]	5045
no. of params refined	367
wt scheme	$1/[\sigma^2(F_o) + (0.20F_o)^2 + 1.0]$
R	0.034
R_w	0.038
goodness of fit	0.37

Experimental Section

Synthesis. Compound **1** was isolated as dark-red crystals in a preparation applying *trans*-$[(NH_3)_2Pt(1\text{-}MeC)_2](NO_3)_2$ and *trans*-$[(NH_3)_2Pd(H_2O)_2](NO_3)_2$ which normally led to *trans*-$[(NH_3)_2Pt(\mu\text{-}1\text{-}MeC^-)_2Pd(NH_3)](NO_3)_2 \cdot 3H_2O$.[4] Conditions were as described in ref 4b, except that the concentration in the present case was higher by a factor of 4. As in the former case, pure crystals of the title compound were obtained only in a late fraction of the crystallization process in low yield (a small percentage), whereas, according to ^{1}H NMR spectroscopy (D_2O), earlier fractions always contained the *trans*-$[(NH_3)_2Pt(1\text{-}MeC)_2](NO_3)_2$ starting compound together with the dinuclear product. ^{1}H NMR spectroscopy did not, however, reveal the presence of $[Pd(NH_3)_4](NO_3)_2$ as found in the crystal. The color of the isolated crystals did not differ from that of *trans*-$[(NH_3)_2Pt(\mu\text{-}1\text{-}MeC^-)_2Pd(NH_3)](NO_3)_2 \cdot 3H_2O$, but elemental analysis showed a considerably higher N content than expected. Anal. Calcd (found) for $C_{10}H_{27}N_{14}O_{11}Pd_{1.5}Pt \cdot 3H_2O$: C, 12.94 (12.7); H, 3.59 (3.0); N, 21.13 (21.1). X-ray crystal structure analysis eventually revealed the true composition.

X-ray Structure Determination. Crystal data and data collection and refinement parameters are summarized in Table 5. A crystal of (**1**), of size 0.25 × 0.30 × 0.25 mm, was used for data collection on a Enraf-Nonius CAD4 automated diffractometer (graphite monochro-

(26) Kuyper, J.; Vrieze, K.; Olie, K. *Cryst. Struct. Commun.* **1976**, *5*, 179.
(27) Kops, R. T.; Schenk, H. *Cryst. Struct. Commun.* **1976**, 5, 193.
(28) Balch, A. L.; Catalano, V. J.; Olmstead, M. M. *Inorg. Chem.* **1990**, *29*, 585.
(29) Balch, A. L.; Catalano, V. J. *Inorg. Chem.* **1991**, *30*, 1302.
(30) Kops, R. T.; Overbeek, A. R.; Schenk, H. *Cryst. Struct. Commun.* **1976**, *5*, 125.
(31) Mc Nair, R. J.; Nilsson, P. V.; Pignolet, L. H. *Inorg. Chem.* **1985**, *24*, 1935.
(32) Yip, H.-K.; Che, C.-M.; Peng, S.-M. *J. Chem. Soc., Chem. Commun.* **1991**, 1626.
(33) Yip, H.-K.; Lin, H.-M.; Wang, Y.; Che, C.-M. *J. Chem. Soc., Dalton Trans.* **1993**, 2939.
(34) Ghilardi, C. A.; Mealli, C.; Midollini, S.; Orlandini, A.; Proserpio, D. M.; Cinquantini, A., Zanello, P. *Struct. Chem.* **1990**, *1*, 441.

mator and Mo Kα radiation). Intensity data were collected with $\omega-2\theta$ scans at room temperature, scan range of $0.7 + 0.35$ (tan θ)°. Intensities were corrected for Lorentz–polarization effects and for absorption *via* empirical ψ scan method (% transmission max 99.4 and min 87.4). No correction for secondary extinction was applied. Three standard reflections, monitored every 180 min, showed no intensity decay. A total of 6899 reflections were measured (octants collected $\pm h,\pm k,+l$), of which 5045 independent reflections [$I > 3\sigma(I)$] were used for solving the structure. Positions of Pt and Pd were determined by conventional Patterson method. All remaining non-H atoms were determined using subsequent Fourier maps. All non-H atoms were anisotropically refined through full-matrix least-squares method. The contributions of H atoms (except those of water molecules) were included in final refinements at fixed calculated positions (C–H bond distance = 0.95 Å, $B = 1.3B_{eq}$ of corresponding bonded atom). The minimum and maximum peak in a ΔF map, −0.28/+2.15 e Å^{-3} (close to Pt). Scattering factors were taken from ref 35. Calculations were carried out on a μVAX 2000 computer using the Enraf-Nonius CAD4 system of programs.[36]

Computational Details. All the MO calculations were of the extended Hückel type[14] (EHMO) using a weighted-modified Wolfsberg–Helmholtz formula[37] and standard atomic parameters.[38] The 3D drawings and correlation diagrams were performed with the program CACAO (computer aided composition of atomic orbitals).[39] Although all the models were idealized, the geometries adopted were the closest to the experimental structures.

Acknowledgment. This work was supported by the Deutsche Forschungsgemeinschaft and CNR and MURST, Rome. C.M. aknowledges the contribution of Progetto Finalizzato Chimica Fine II. We thank G. Fusch for providing details on the Pt, Cu compounds.

Supplementary Material Available: Lists of structure factors, anisotropic thermal parameters for non-hydrogen atoms, positional parameters for hydrogen atoms, complete bond lengths and angles, distances, overlap populations and net atomic charges matrices (5 pages). Ordering information is given on any current masthead page.

IC9407003

(35) *International Tables for X-ray Crystallography*; Kynoch: Birmingham, England; 1974; Vol. IV.
(36) Frenz, B. A. *Enraf-Nonius Structure Determination Package*; Frenz, B. A. and Associates: College Station, TX; and Enraf-Nonius; Delft, The Netherlands.
(37) Ammeter, J. H.; Bürgi, H.-B.; Thibeault, J. C.; Hoffmann, R. *J. Am. Chem. Soc.* **1978**, *100*, 3686.
(38) Alvarez, S. *Tables of Parameters for Extended Hückel Calculations;* Departamento de Quìmica Inorganica, Universitàt de Barcelona: Barcelona, Spain, 1989.
(39) Mealli, C.; Proserpio, D. M. *J. Chem. Educ.* **1990**, *67*, 399.